Electrochemical characterization of galvanically coupled single phases and nanocrystalline NdFeB-based magnets in NaCl solutions

A.A. EL-MONEIM[1,2] and A. GEBERT[2,*]
[1]*Physical Chemistry Department, National Research Center, Cairo, Egypt*
[2]*Institute for Solid State and Materials Research Dresden, PO Box 270016, D-01171Dresden, Germany*
(*author for correspondence, fax: +49 (0)351 4659 541, e-mail: a.gebert@ifw-dresden.de)

Abstract

Galvanic interaction between intermetallic phases occurring in NdFeB-based permanent magnets was investigated for the purpose of understanding the electrochemical behaviour of nanocrystalline hot pressed $Nd_{14}Fe_{80}B_6$ and $Nd_{12}Dy_2Fe_{73.3}Co_{6.6}Ga_{0.6}B_{5.6}$ magnets in 0.5 M NaCl solution of pH 8.4. The microstructure of multiphase nanocrystalline magnets was characterized using XRD, SEM and EDX techniques. The electrochemical behaviour was assessed using zero resistance amperometry and potentiodynamic polarization measurements. From the electrochemical data obtained, it was concluded that the Nd-rich phase/ferromagnetic (ϕ)- phase couple generated the highest galvanic current density. The strength of the galvanic coupling effect was typically controlled by the oxidation rate of Nd-rich phase, which is the least polarizable. Pitting and intergranular corrosion were detected on the surface of nanocrystalline magnets and found to be dependent on each other, since intergranular corrosion processes nucleated on the pit walls and propagated from there. Crystallographic tunneling was found to be the way of both pit and intergranular corrosion propagation. Co and Ga additions generally increase localized corrosion resistance of NdFeB-based magnets due to the significant reduction in the strength of galvanic coupling effect between magnet phases.

1. Introduction

NdFeB-based magnets find a rapidly growing variety of applications, because of their outstanding magnetic properties, like high remanence, coercivity and energy products [1]. On the other hand, the corrosion resistance of those magnets is one of the key parameters in assessing their applicability. NdFeB magnets are very sensitive to climatic and corrosive environments. The poor corrosion resistance of these magnets is due to their high content of Nd and the coexistence of several phases in the microstructure, which are necessary to ensure the required magnetic properties [2]. The microstructure comprises of the ferromagnetic matrix-phase or Φ-phase ($Nd_2Fe_{14}B$) surrounded by intergranular regions consisting of B-rich ($Nd_{1+\varepsilon}Fe_4B_4$) and Nd-rich ($Nd_4Fe$) phases [3]. Other beneficial phases stabilized by alloying additions such as Al, Co, Cu, Cr, Mo, Nb and Ga may also be present [2–4]. Meanwhile, the volume fraction of the ferromagnetic matrix phase in sintered microcrystalline magnets is about 84%, while those of Nd and B-rich phases are 14 and 2%, respectively. In hot pressed nanocrystalline magnets, the total volume fraction of intergranular phases is reduced to about 13% due to the low Nd content in these types of magnets [3].

Hence, this significant variation in the chemical composition and volume fraction of magnet phases with large electrochemical potential differences between them present an obvious threat of galvanic corrosion, which has not been fully clarified, yet.

So far, the majority of corrosion tests have been performed on single phases of the magnet and microcrystalline permanent magnets prepared by sintering rather than on nanocrystalline magnets prepared by nonequilibrium powder preparation techniques and by subsequent hot pressing. Tests have been conducted in humid atmospheres [3] and electrolytes such as H_3PO_4, H_2SO_4, Na_2HPO_4 and Ringers solution under deaerated conditions [3, 5–7]. According to Sugimoto [8], the susceptibility of single phases to dissolution in acidic media increased in the following order: $Nd_2Fe_{14}B < Nd_4Fe < Nd_{1+\varepsilon}Fe_4B_4$. Schultz et al. [3] referred to some other order in humid atmosphere: $Nd_2Fe_{14}B < Nd_{1+\varepsilon}Fe_4B_4 < Nd_4Fe$. A third order, proposed by Bala et al. [9], was $Nd_{1+\varepsilon}Fe_4B_4 < Nd_2\text{-}Fe_{14}B < Nd_4Fe$ in 0.5 M Na_2SO_4 solutions of several pH values. In the view of these facts, the Nd–rich intergranular phase is generally considered as local anode with respect to the matrix phase. Consequently, the corrosion mechanism of NdFeB magnets in the

above electrolytes was described as preferential dissolution of intergranular phases followed by the separation of ferromagnetic grains from magnet surface before their dissolution [3, 10–13].

Since the corrosion of NdFeB magnets is of concern in industrial and marine environments as well as in automotive environment containing de-icing salts, tests performed in aerated, neutral electrolytes such as Na_2SO_4 and NaCl will probably be more relevant to the actual service conditions. The corrosion behaviour of NdFeB magnets and their constituent phases in environments containing chloride ions has not been documented in detail. The aim of this study is to characterize the electrochemical behaviour of uncoupled and galvanically coupled single phases occurring in NdFeB-based magnets in weakly alkaline solution containing chloride ions. A deeper knowledge of these electrochemical phenomena, such as pitting and galvanic corrosion, contributes to a more comprehensive understanding of the overall complex corrosion process of hot pressed nanocrystalline NdFeB magnets with and without Co and Ga additions.

2. Experimental details

The as-cast material of the three phases generally occurring in NdFeB-based magnets were received from the Department of Chemistry of the Technical University of Czestochowa, Poland. Microstructural analysis and chemical composition of these phases were verified and identified in detail elsewhere [3, 9, 14]. Additionally, two types of bulk material prepared from commercial nanocrystalline melt-spun powders (ribbon flakes) of the nominal compositions $Nd_{14}Fe_{80}B_6$ and $Nd_{12}Dy_2Fe_{73.3}$-$Co_{6.6}Ga_{0.6}B_{5.6}$ with commercial names MQP-A and MQU-G (from Magenquench Int.), respectively, were used as typical examples for permanent magnets. The powders were hot pressed in vacuum at 700 °C, applying a pressure of 150 MPa to obtain a highly densified magnet with diameter of 8 mm and a height of 8 mm. Characterization of grain sizes, shapes and phase distribution were carried out on hot pressed magnets using scanning electron microscopy (SEM, Jeol JSM-6400) complemented with energy dispersive X-ray analysis (EDX) (Noran-Voyager).

Singles phases and permanent magnets were cut and embedded in epoxy resin and mechanically polished up to 1 μm using diamond paste. After polishing, test specimens were ultrasonically cleaned with ethanol and dried in air. Electrochemical measurements were performed in aerated borate buffer solution (0.075 M $Na_2B_4O_7$–0.3 M H_3BO_4) with pH 8.4 containing 0.5 M NaCl.

For time dependent galvanic corrosion measurements, a nonperturbative electrochemical technique such as zero-resistance amperometry (ZRA) is required. A detailed description of this type of measurement is given elsewhere [15, 16]. By inserting a zero-resistance amp-

erometer in the electrical circuit that connects two single phases, it was possible to measure the galvanic current between phases and simultaneously, the galvanic potential of the pair was registered against a saturated calomel electrode (SCE) as a reference electrode. The galvanic current and potential was measured at sampling rate of 1 point s^{-1}. The ZRA was programmed to record 600 points potential and current plots for each hour of total 24 h measurement duration.

Polarization measurements were generated using a Solartron electrochemical interface, which also acted as ZRA. The auxiliary electrode was platinum. Potential sweep rate was 1 mV s^{-1}. After open circuit immersion or polarization, investigations using light optical microscopy and scanning electron microscopy (SEM) were performed on the samples in order to examine and locate pits and/or intergranular corrosion phenomena.

3. Results and discussion

3.1. Microstructural characterization of nanocrystalline magnets

Figure 1(a) and (b) show SEM micrographs in the backscattered electron mode of polished sample surfaces for hot pressed $Nd_{14}Fe_{80}B_6$ (MQP-A) and $Nd_{12}Dy_2$-$Fe_{73.3}Co_{6.6}Ga_{0.6}B_{5.6}$ (MQU-G) magnets, respectively. In these micrographs, finely dispersed clusters and continuous regions of white contrast with a thickness of about 1~3 μm at the ribbon flake boundaries were identified by EDX analysis as Nd-rich region. Gray contrasts represent regions mainly consisting of the ferromagnetic matrix phase. Detailed analysis using TEM revealed that the grains of the matrix phase with sizes in the range of 50–100 nm are surrounded by a thin (1–5 nm) continuous network of Nd-rich grain boundary phase [17, 18].

Figure 2 shows a typical SEM micrograph of a fractured surface of a hot pressed $Nd_{14}Fe_{80}B_6$ (MQP-A) sample. As seen, the microstructure is very fine with homogeneous grain size distribution. No significant change in the microstructure is observed for a sample with Co and Ga additions, though the mean grain size of the matrix phase is slightly reduced from 100 to 60 nm [19].

EDX analysis for the NdFeB magnet (MQP-A) revealed that the concentration of neodymium in the Nd-rich regions (corresponding to Figure 1(a)) at flakes boundaries is about 93 at %. The combined addition of 6.6 at % Co and 0.6 at % Ga (MQU-G) results in a strong depletion in the total amount of rare earth (RE)-elements in these regions (67 at %) as indicated in Table 1 [11]. Therefore, it is reasonable to assume that minor addition of Ga besides Co generate new intergranular phases. This agrees well with earlier investigations by Szymura et al. [20], Yamamoto et al. [21] and Fidler et al. [22] of sintered microcrystalline permanent magnets, where the formation of $Nd_{16}Fe_{13}Ga$, $Nd_3(Ga,Fe)$, $Nd_5(Ga,Fe)_3$, and Nd_3Co intergranular
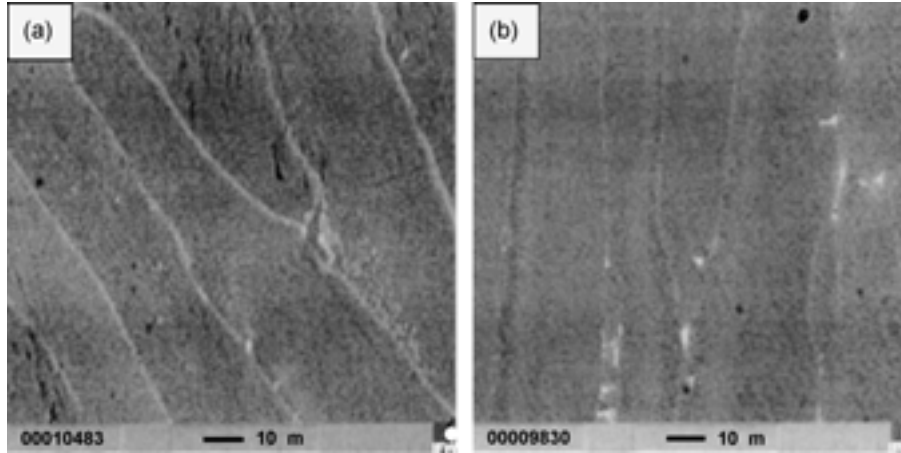
Fig. 1. SEM micrographs (backscattered electron mode) of polished surfaces of hot pressed (a) NdFeB (MQP-A) and (b) NdDyFeCoGaB (MQU-G) magnets.
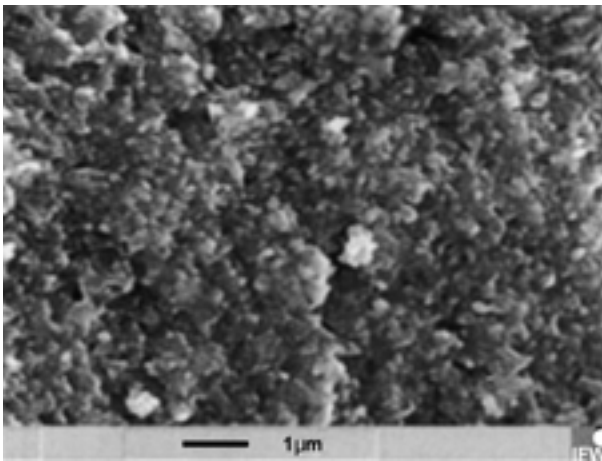

Fig. 2. SEM micrograph of a fractured surface of a hot pressed MQP-A magnet.

Table 1. Concentration of magnets components (at %) (EDX analysis) at triple points of Nd-rich regions at ribbon flakes boundaries

	Nd	Dy	Fe	Co	Ga
MQP-A*	92.6		7.40		
MQU-G†	60.10	6.15	6.40	14.11	13.18

* See Figure 1(a).
† See Figure 1(b).

type phases was found. Furthermore, it is detected that Co and Ga additions do not influence the content of RE-elements in the matrix phase or modify its structure significantly. In this concern, Schultz et al. [3] reported that partial substitution of Fe with Co, Al and Ga in hot pressed nanocrystalline magnets prepared by hydrogen disproportionation desorption reaction (HDDR) significantly reduces the electrostatic surface potential difference between matrix and intergranular phases measured in air by means of an AFM (atomic force microscope) using it as an electrostatic force microscope (EFM). This indicates that, Co and Ga additions reduce the strength of galvanic interaction between the magnet phases.

3.2. Electrochemical characterization

3.2.1. Electrochemical characterization of uncoupled and two galvanically coupled single phases

Figure 3(a–c) demonstrate the superposition of polarization curves of two single phases, with electrode surface area ratio (1:1), traced after 1 h immersion under free corrosion condition in 0.5 M NaCl solution of pH 8.4. In these Figures, the corrosion current density (i_{corr}) of uncoupled phases is determined at the intersection point of anodic and cathodic Tafel lines with the vertical through the corrosion potential (E_{corr}). In the light of mixed potential theory, the intersection point of polarization curves of two different phases defines the mixed potential (E_{couple}) and the galvanic current density (i_{couple}).

For uncoupled single phases, it is seen in Figure 3 that the Nd-rich phase (Nd-phase) dissolves actively, whereas the ferromagnetic phase (ϕ-phase) and the B-rich phase (B-phase) are spontaneously passive and suffer from pitting attack with anodic polarization in 0.5 M NaCl solution of pH 8.4. In addition, the polarization plots show that the corrosion potential (E_{corr}) of the Nd-rich phase is far more negative than those of ferromagnetic and B-rich phases. Meanwhile, i_{corr} values of uncoupled single phases reveal that the electrochemical activity increases in the following order: Φ-phase < B-rich phase < Nd-rich phase (Table 2). Therefore, the galvanic interaction between these phases is clearly posed.

On the other hand, the polarization curves (Figure 3(a)) of ferromagnetic and B-rich phases are very close to each other. Therefore, no significant effect is noticed in their polarization behavior when they galvanically interact as obvious from the comparison of (i_{corr}) and (E_{corr}) values for the single phases and (i_{couple}) and (E_{couple}) values for the coupled pair (Table 2). In
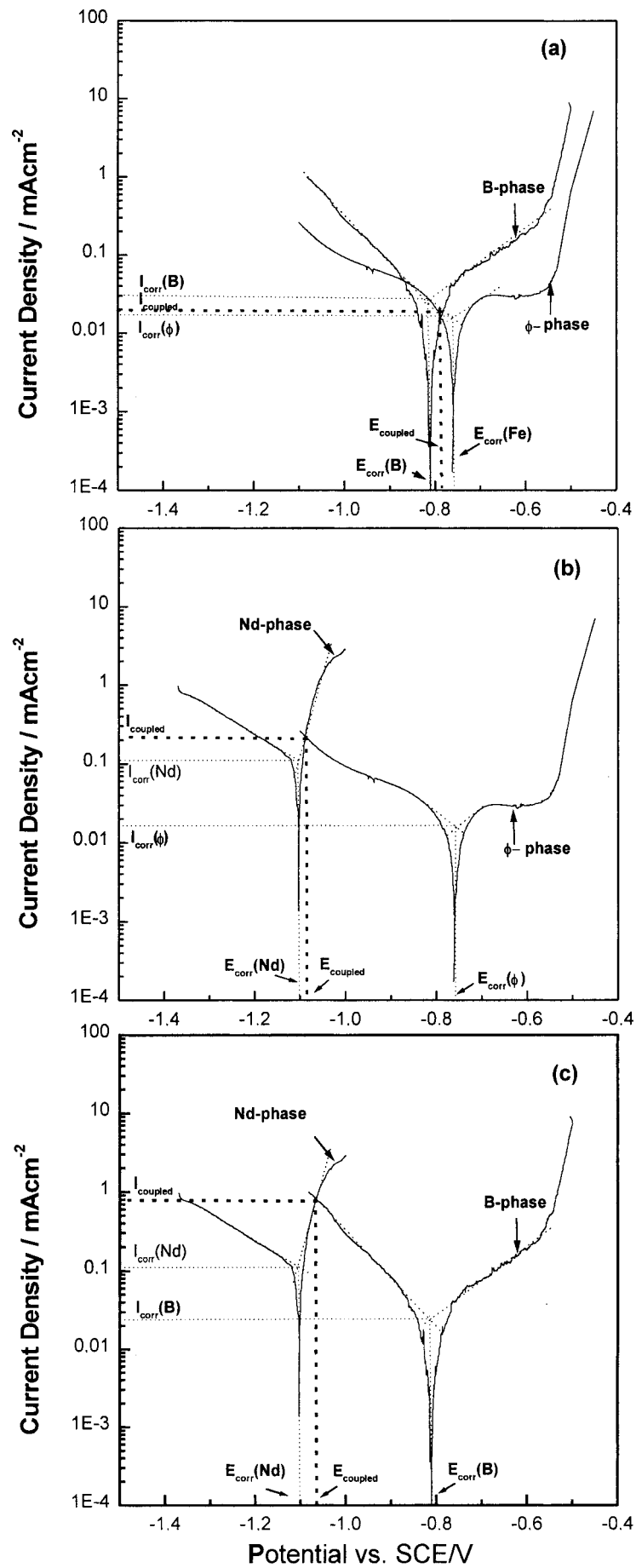
Fig. 3. Potentiodynamic polarization curves (1 mV s⁻¹) for two single phases measured in aerated 0.5 M NaCl solution of pH 8.4: (a) Nd-rich phase/ferromagnetic (ϕ)-phase, (b) Nd-rich phase/B-rich phase, (c) ferromagnetic (ϕ)-phase/B-rich phase.

Table 2. Comparison of E_{corr} and i_{corr} values of uncoupled magnet phases with E_{couple} and i_{couple} values obtained from superposition of polarization curves of two coupled single phases of NdFeB magnets in aerated 0.5 M NaCl solution of pH 8.4. E_{couple} and i_{couple} values obtained from ZRA measurements after immersion for 1 and 24 h are also shown for comparison

	Potentiodynamic polarization				ZRA			
	E_{corr}, 1 h /V vs SCE	i_{corr}, 1 h /mA cm^{-2}	E_{couple}, 1 h /V vs SCE	i_{couple}, 1 h /mA cm^{-2}	E_{couple}, 1 h /V vs SCE	i_{couple}, 1 h /mA cm^{-2}	E_{couple}, 24 h /V vs SCE	i_{couple}, 24 h /mA cm^{-2}
Nd-phase/Φ-phase	−1.105	0.123	−1.092	0.233	−1.060	0.239	−0.988	0.094
Nd-phase/B-phase	−0.811	0.026	−1.069	0.785	−1.038	0.440	−0.988	0.043
B-phase/Φ-phase	−0.762	0.0187	−0.774	0.012	−0.748	0.015	−0.699	0.011

contrast, the dissolution current density (i_{corr}) of the Nd-rich phase at E_{corr} of about −1.105 V vs SCE increases from 0.123 mA cm^{-2} to 0.234 and 0.785 mA cm^{-2} (i_{couple}) at mixed potentials (E_{couple}) corresponding to −1.092 and −1.069 V vs SCE upon coupling with the ferromagnetic ϕ-phase (Figure 3(b)) and the B-rich (Figure 3(c)) phase, respectively. Consequently, the strength of the galvanic coupling effect of all these pairs of single phases in weakly alkaline chloride solution is the highest for the Nd-rich phase/B-rich phase couple and both, the ferromagnetic phase and the B-rich phase are cathodically polarized when galvanically coupled with the Nd-rich phase, which acts as a local anode.

For time-resolved characterization of the galvanic corrosion behaviour of all pairs of single phases, ZRA measurements were carried out under the experimental conditions previously described. Due to the significant fluctuations of both, galvanic potential and current density values in the present investigation, the sampled potential and current density data of each time record were statistically analysed and expressed in terms of mean and standard deviation values. These values generally give a basic correlation between the intensity of potential and current fluctuations and rate and mode of corrosion attack [16, 23, 24]. Figure 4(a) and (b) presents the estimated mean galvanic current density
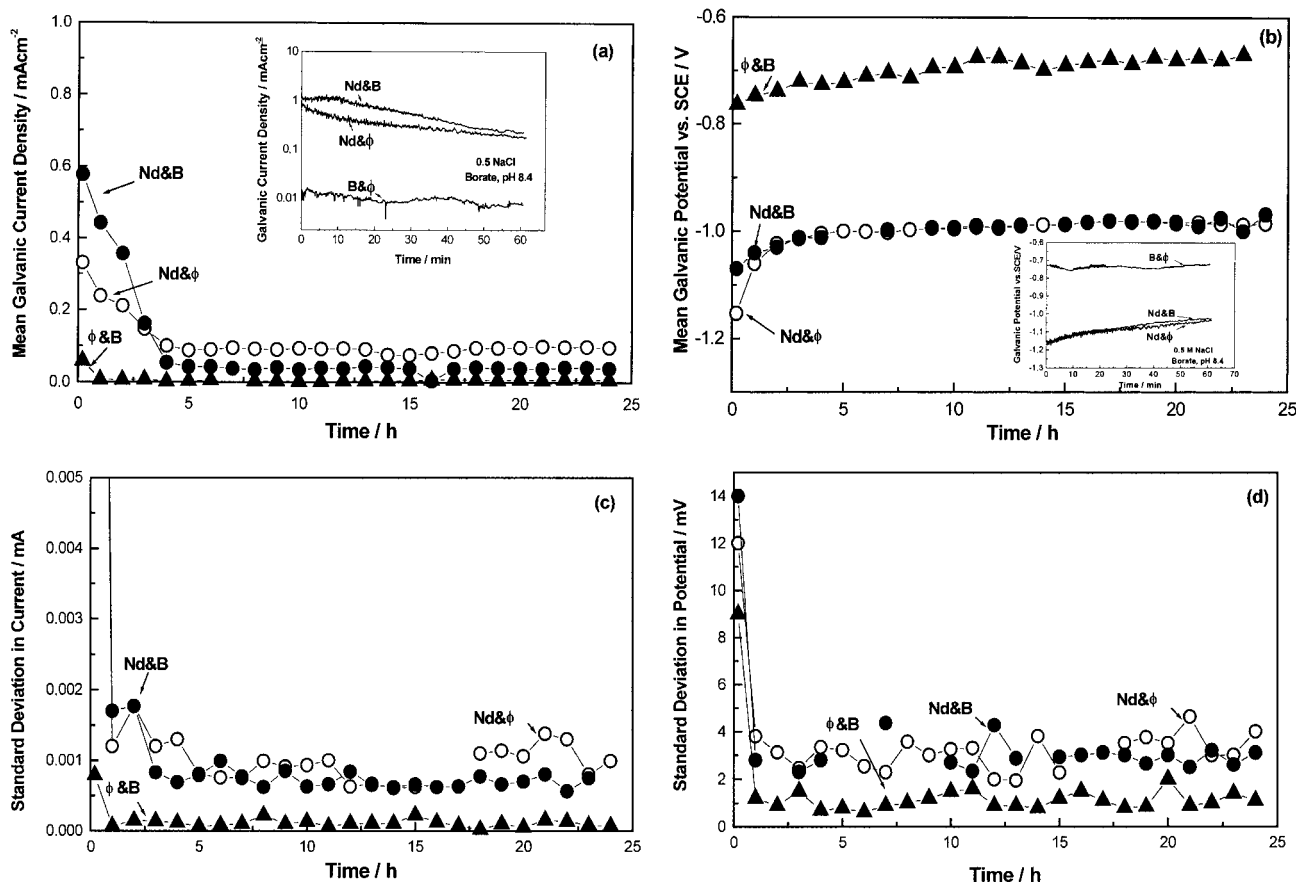

Fig. 4. Mean galvanic current density (a) and mean galvanic potential (b) of all pairs of coupled phases in 0.5 M NaCl solution of pH 8.4 determined by the ZRA method. Standard deviations of current density (c) and potential (d) data of all pairs of coupled phases are also shown for comparison.

and potential values for 24 h measurement duration in aerated 0.5 M NaCl solution of pH 8.4 for the surface area ratio (1:1) of coupled phases, respectively. Standard deviation values due to potential and current fluctuations are also presented in Figure 4(c) and (d), respectively. The inserts of (a) and (b) show typical examples of simultaneously measured galvanic current densities and potentials during the first hour of the 24 h of measurement.

In Figure 4(a) it is clearly seen that, the mean values of galvanic current densities generally attain their steady states after about 3 h immersion for all coupled pairs. It is also worth noting that the highest mean current density values during the initial 3 h are that of the Nd-rich phase/B-rich phase couple. These results, particularly those obtained after 1 h immersion of pairs, correlate with the results gained from slowly measured potentiodynamic polarization curves, seen in Figure 3 (and Table 2). During the steady state, the highest mean current density values are obtained from Nd-rich phase/ ferromagnetic phase couple. The reason for this alteration in the electrochemical behavior with time is not clear, yet. Standard deviation results shown in Figure 4(c) are well correlated with the results in Figure 4(a), that is, the highest standard deviations values coincide with the highest corrosion rates originated from galvanic coupling of the Nd-rich phase with the ferromagnetic and B-rich phases. Meanwhile, all galvanic potential values which were determined by both types of measurements (potentiodynamic polarization and ZRA) are summarized in Table 2. For Nd-rich phase/ferromagnetic phase and Nd-rich phase/B-rich phase couples (E_{couple}) values are generally located in the close proximity of the (E_{corr}) value of the Nd-rich single phase. Hence, the overall galvanic reaction in these coupled systems seems to be mainly governed by the anodic oxidation of the Nd-rich phase, which is the highest active and least polarizable.

3.2.2. Electrochemical characterization of three coupled phases

In general, at the mixed potential (E_{couple}) of multiphase material systems the conditions $\sum i_{\text{anode}} = \sum i_{\text{cathode}}$ has to be fulfilled to maintain charge neutrality [25]. For the magnets single phases this condition can be fulfilled if the Nd-rich phase acts as the anode and both nobler phases (i.e., B-rich and ferromagnetic phases) act as the cathodes. Accordingly, the mixed potential (E_{couple}) for three coupled phases is a consequence of $i_{\text{Nd-rich phase}} = i_{\text{B-rich phase}} + i_{\text{ferromagnetic phase}}$. Under this condition and as shown in Figure 5(a), the estimated value of (E_{couple}) for the three-phase composition with a surface area ratio (1:1:1) is −1.057 V vs SCE. This value is nearby the intersection of polarization curves of Nd-rich and B-rich phases, because at the mixed potential the B-rich phase ($i_{\text{galvanic (Nd-rich/B-rich)}}$ or $i_{\text{cathodic(B-rich phase)}} = -0.798$ mA cm^{-2}) contributes much more to the sum of the cathodic current densities than the ferromagnetic phase ($i_{\text{galvanic (Nd-rich/ferromagnetic)}}$ or
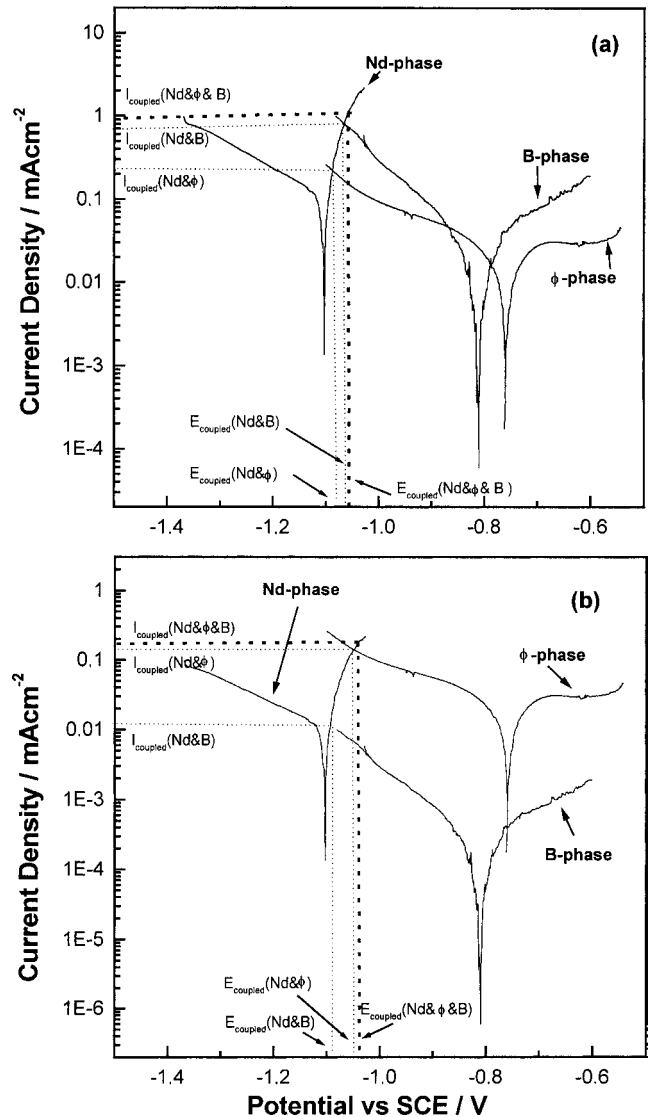

Fig. 5. Potentiodynamic polarization curves for three-phase composition with surface area ratio of (a) 1:1:1 (B-rich phase:Nd-rich phase:Φ-phase) and (b) 1:10:100 in 0.5 M NaCl solution of pH 8.4.

$i_{\text{cathodic}(\phi\text{-phase})} = -0.233$ mA cm^{-2}, see Table 3). Because of polarization, the anodic current density or total galvanic current density for the Nd-rich phase corresponds to $i_{\text{anodic}} = +1.028$ mA cm^{-2}. This value is related to the surface area of the corroding Nd-rich single phase. However, the surface area of Nd-rich single phase occupies only a third of the entire electrode surface (A) for the phase composition (1:1:1) ($A = A_{\text{B-rich}} + A_{\text{Nd-rich}} + A_{\text{ferromagnetic}}$). Therefore, all current densities related to the entire surface are lowered by a factor of 1/3 ($i_{\text{anodic}} = +0.343$ mA cm^{-2}), as seen in Table 3.

On other hand, the entire surface area related to polarization curves allows comparison with other phase composition like (1:10:100) ($A = A_{\text{B-rich}} + A_{\text{Nd-rich}} + A_{\text{ferromagnetic}}$). With respect to the multiphase permanent magnet microstructure, this ratio seems to be more realistic than the ratio (1:1:1) since Nd- and B-rich phases occupy only small intergranular regions around the large volume fraction of the ferromagnetic grains, as

Table 3. Anodic dissolution current density (i_{anode}) and corresponding cathodic current densities ($i_{cathode}$) for NdFeB magnets derived from the superposition of three coupled single phases with different surface area ratio in 0.5 M NaCl solution of pH 8.4

	Current density /mA cm^{-2} Related to single phase area			Related to entire surface		
	i_{anodic} of Nd-rich phase	$i_{cathodic}$ of B-rich phase	$i_{cathodic}$ of Φ-phase	i_{anodic} of Nd-rich phase	$i_{cathodic}$ of B-rich phase	$i_{cathodic}$ of Φ-phase
Ratio of area 1:1:1*	+ 1.028	−0.798	−0.233	+ 0.343	−0.266	−0.077
Ratio of area 1:10:100*	+ 1.440	−0.100	−1.330	+ 0.144	−0.011	−0.133

* B-rich:Nd-rich:Φ-phase.

already discussed. Consequently, the polarization curves of B- and Nd-rich phases in Figure 5(a) have to be multiplied by 1/100 and 1/10, respectively, to obtain polarization curves related to the entire surface of the multiphase composition (1:10:100) (Figure 5(b)). The estimated mixed potential values for the new ratio (i.e., 1:10:100) is −1.045 V vs SCE, which occurs also in vicinity of the (E_{corr}) value of the Nd-rich phase and even closer to the mixed potential of Nd-rich phase/ferromagnetic phase coupled pair (Table 2). In addition, it is only slightly more positive than the mixed potential corresponding to the area ratio (1:1:1). This demonstrates again that, the anodic oxidation of the Nd-rich phase is the dominating process of the overall surface reaction of such a three-phase system in a weakly alkaline chloride solution of pH 8.4. In contrast, Barkleit et al. [25] have shown that, the estimated mixed potential for the same coupled systems in 0.1 M H$_2$SO$_4$ solution is generally located near the (E_{corr}) value of the ferromagnetic phase. This is an indication that the overall surface reaction of such a system in acidic environment is more under cathodic regime.

Furthermore, in the chloride-containing solution the dissolution current density related to the entire surface of the three-phase composition (1:10:100) rises from 0.012 mA cm^{-2} at the corrosion potential of the Nd-rich phase to i_{anodic} = + 0.144 mA cm^{-2} at the mixed potential (E_{couple}) (Nd, ϕ and B; Table 3). But the anodic dissolution current density (i_{anodic}) only related to the small area of corroding Nd-rich phase, as it may occur in the intergranular regions of a permanent magnet, is higher by factor 10 (i_{anodic} = + 1.440 mA cm^{-2}). Meanwhile, the corresponding cathodic current density related to the entire surface is generally distributed between the ferromagnetic phase (−0.133 mA cm^{-2}) and the B-rich (−0.011 mA cm^{-2}) phase (Table 3) and is mainly related to reduction of water or dissolved oxygen.

3.2.3. *Electrochemical characterization of nanocrystalline magnets*

Analysis of the data in Table 3 reveals that, the estimated current density values for the Nd-rich phase upon coupling seem to be high enough to initiate and develop localized attack on the surface of NdFeB-based magnets in weakly alkaline solution containing chloride ions. This gives rise to more detailed studies on the pitting corrosion behavior of permanent magnets, though localized corrosion processes are very complex and thus, hardly to describe in detail for those multiphase materials. The following investigations aim for comparing the pitting susceptibility of Nd$_{14}$Fe$_{80}$B$_6$ (MQP-A) and Nd$_{12}$Dy$_2$Fe$_{73.3}$Co$_{6.6}$Ga$_{0.6}$B$_{5.6}$ (MQU-G) magnets under the same defined experimental conditions. At first, both types of magnets were immersed in 0.5 M NaCl solution of pH 8.4 for a selected period of 24 h, similarly to [26], for studying the pitting under free corrosion conditions. Within this period, at the open circuit potential (OCP) pitting is revealed only for the MQP-A magnet, whereas the MQU-G magnet did not exhibit local damages. Nevertheless, our in-situ investigations under the same experimental conditions using nondistributive electrochemical noise technique (which is out of the scope of the current article) showed that the incubation periods for pitting initiation on MQP-A and MQU-G magnets are about 12 and 27 h, respectively.

Figure 6(a) and (b) presents light optical microscopy images of the MQP-A magnet surface obtained after 24 h open circuit immersion in 0.5 M NaCl solution with pH 8.4. White thick corrosion product is formed on the surface of the magnet (Figure 6(a)), which when analysed in the SEM with EDX revealed the presence of significant amounts of O, Cl and Nd with traces of Fe. After polishing using 1 μm diamond paste, pronounced pitting attack is noticed along the ribbon flake boundaries of the melt-spun and hot pressed material indicating that Nd-rich regions act as pitting initiation sites, as shown in Figure 6(b). Additionally, the observed pits are significantly ramified presenting an irregular shape. Obviously, at OCP surface precipitates inhibit an ion exchange between the forming pit and the bulk electrolyte and thus, control the kinetics of the pitting process which in result leads to this distinct pit morphology.

Furthermore, the pitting behaviour of the magnets under anodic polarization conditions on a shorter timescale was investigated. Figure 7 shows potentiodynamic cyclic polarization curves for Nd$_{14}$Fe$_{80}$B$_6$ (MQP-A) and Nd$_{12}$Dy$_2$Fe$_{73.3}$Co$_{6.6}$Ga$_{0.6}$B$_{5.6}$ (MQU-G) magnets recorded with 1 mV s^{-1} after 1 h immersion in 0.5 M NaCl solution with pH 8.4. From previous studies [2, 3, 10] it is known that, the overall degradation process of NdFeB-based magnets in humid environments is the consequence not only of electrochemical reactions but
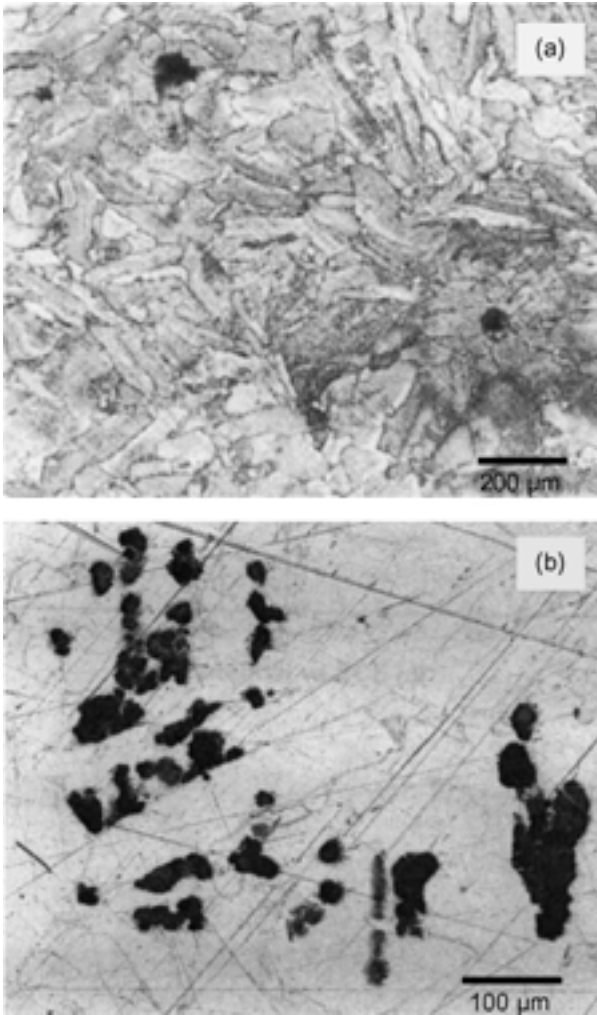
Fig. 6. Light optical micrographs of a MQP-A magnet surface after immersion for 24 h under free corrosion condition in 0.5 M NaCl solution of pH 8.4: (a) as-corroded surface and (b) surface after short polishing.
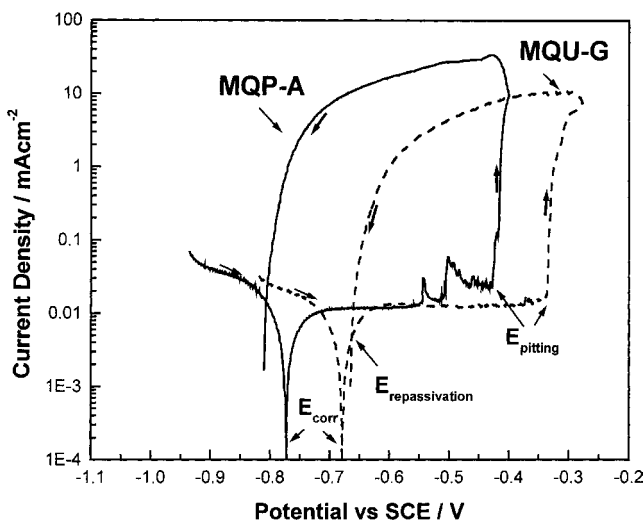

Fig. 7. Potentiodynamic polarization curves (1 mV s^{-1}) for MQP-A and MQU-G magnets in aerated 0.5 M NaCl solution of pH 8.4.

also of mechanical degradation. In order to minimize the probability of occurrence of those mechanical degradation processes during the experiment, a potential scan-rate somewhat faster than the scan-rate recommended by the ASTM society for studying pitting processes of metals and alloys, $\leqslant 0.5$ mV s^{-1}, was chosen. As seen, both magnets are spontaneously passive and suffer from pitting corrosion with anodic polarization at higher potential. Nevertheless, the NdFeB-based magnet with Co and Ga (MQU-G) addition exhibits better resistance to pitting corrosion under the given polarization conditions.

In general, $\Delta E_i = E_{\text{repassivation}} - E_{\text{corr}}$ and $\Delta E_g = E_{\text{pitting}} - E_{\text{repassivation}}$ values can serve as criteria for evaluating the pitting susceptibility of an electrode. In this concern, E_{pitting} is a critical potential value beyond which ($E \geqslant E_{\text{pitting}}$) pit propagation occurs (i.e., formation of stable pit) indicated by a steep rise if the current density. At $E < E_{\text{pitting}}$ stable pits cannot be formed. $E_{\text{repassivation}}$ is a potential value for which at $E \geqslant E_{\text{repassivation}}$ pits can initiate (i.e., formation meta-stable pit or pit embryo), but at $E < E_{\text{repassivation}}$ the material remains passive. Accordingly, a more negative value of ΔE_i indicates the higher affinity of an electrode for pit initiation under free corrosion condition. Furthermore, a larger ΔE_g value or area under the hysteresis loop obtained during slow cycling polarization refers to a high rate of pit propagation or pit growth on the electrode surface [27]. Fundamental papers of Leckie and Uhlig [26] and Heusler and Fischer [28] pointed out that pitting processes are strongly kinetically controlled. This is expressed, for example, in a significant incubation time for pit initiation. Thus, determination of critical pitting potentials must be performed with the slowest possible potential shift (scan rate) to realize quasi-stationary conditions. In general, the potential scan rate affects both the critical pitting and repassivation potential. An increase in scan rate shifts the pitting potential to move noble values and the repassivation potential to less positive potentials. However, the slight increase in the scan rate from 0.5 mV s^{-1} to 1 mV s^{-1} will not affect the reliability of our experiment for comparison of the pitting corrosion behaviour of MQP-A and MQU-G magnets.

By analysis of curves shown in Figure 7, the estimated values of ΔE_i and ΔE_g are -0.03 and 0.38 V vs SCE for the MQP-A magnet and 0.02 and 0.32 V vs SCE for the MQU-G magnet, respectively. It follows from the above discussion that the combined addition of Co and Ga diminishes both, the pit initiation and the pit propagation tendency on the surface of a NdFeB-based magnet. Co and Ga additions do not lead to a significant change in the mean grain size and phase distribution of the NdFeB-based magnets, but they are mainly enriched in the intergranular regions. Consequently, the Nd content of these regions is significantly reduced [21, 22]. Also, they do not have a passivating character in the investigated medium [29]. The reduction of the strength of the galvanic coupling effect between matrix and intergranu-

lar phases by alloying addition seems to be responsible for the higher pitting corrosion resistance of the MQU-G magnet.

Figure 8(a) presents a SEM micrograph of a pit developed on the surface of a MQP-A magnet after potentiodynamic polarization up to a potential which is 0.1 V vs SCE more positive than the pitting potential $E_{pitting}$. The morphology of local damages formed under anodic polarization conditions is different from that observed after long-term immersion at OCP (compare Figure 6). It can be seen that pitting, as well as local intergranular corrosion attack, developed. It is also worth noting that, those surface regions where pits did not develop, also did not enable intergranular corrosion to develop and remained unattacked. Figure 8(b) and (c) shows SEM images at higher magnifications in which it can be seen that pitting is very extensive and that micro- and nano-sized crystallographic tunnels are conspicuous. When some of these tunnels penetrate grain boundaries, intergranular corrosion starts and tunneling supports the intergranular corrosion processes. In other words, crystallographic tunneling seems to be decisive for pitting and intergranular corrosion propagation and this indicates that the two forms of localized corrosion are strongly dependent on each other.

The question remains, how pitting and intergranular corrosion are interrelated. Across the potentiodynamically corroded surface of the MQP-A magnet many voluminous and volcano shaped corrosion products were observed. The corrosion product is characterized with a hole in their centre, which is very fragile and collapses when exposed in the vacuum chamber of the SEM (Figure 9). Beneath each of these visible corrosion products a pit exists. Thus, the growing pit was isolated from the environment by deposited corrosion products
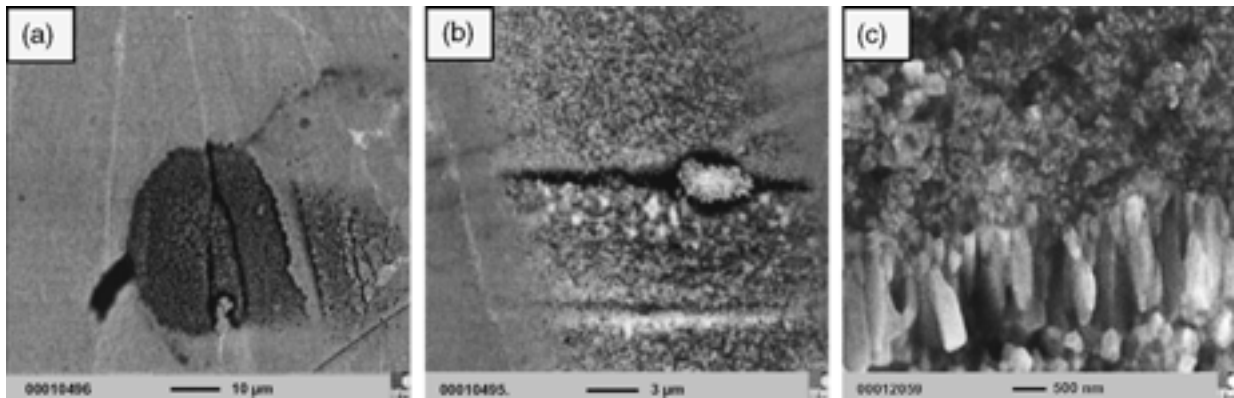

Fig. 8. SEM micrographs of a pit generated in 0.5 M NaCl solution of pH 8.4 on a MQP-A magnet surface (ultrasonically cleaned) by potentiodynamic polarization up to a potential 0.1 V vs SCE more positive than the pitting potential: (a) and (b) show microscopic observations with low and high magnification and (c) SEM micrograph taken inside a pit.
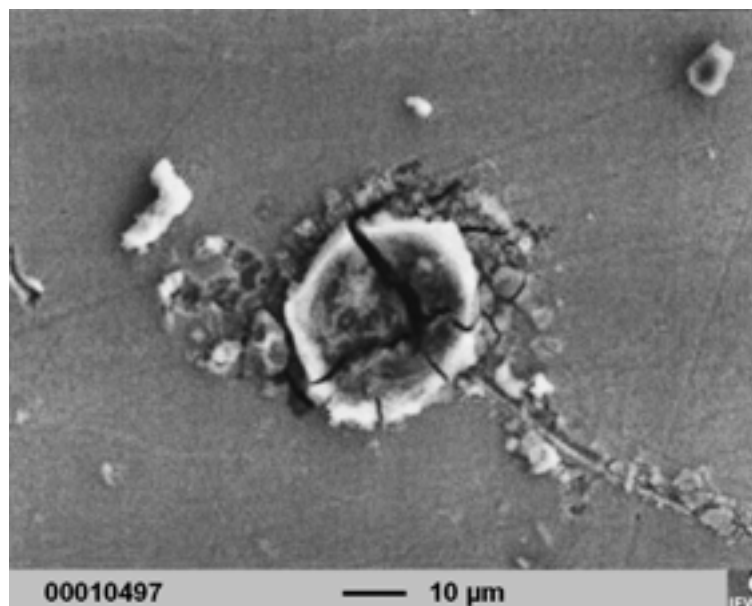

Fig. 9. SEM micrographs of a pit generated on a MQP-A magnet surface by potentiodynamic polarization up to a potential 0.1 V vs SCE more positive than the pitting potential.

and thus, the electrolyte in the pit became more and more acidic with high chloride ion concentration. Indeed, local acidification is one of the possible mechanisms of accelerated pit propagation [30, 31]. In this acidified environment, pits grow on the magnets surface through the micro- and/or nano-sized tunnels and penetrate along grain and flake boundaries. Hence, intergranular corrosion starts.

To confirm the above statement, MQP-A and MQU-G magnets surfaces were inspected with SEM after 10 min immersion in 0.001 M HCl solution, which may simulate a typical pit environment. It is clearly seen in Figure 10(a) and (b) that the Nd-rich region along flake boundaries and intergranular regions of the MQP-A magnet are preferentially attacked (Figure 10(a)), though the MQU-G magnets surface exhibits much less intergranular corrosion damage Figure 10(b). This observation confirms the above view and indicates the beneficial effect of Co and Ga addition in retarding the propagation of pitting and intergranular corrosion. Therefore, it can be postulated that acidic environment is essential to stimulate the intergranular corrosion for NdFeB-based magnets. If there are no occluded cells (such as pits), and if the bulk environment is weakly alkaline, then intergranular corrosion should not be pronounced.

4. Conclusions

The electrochemical behavior of uncoupled and two or three galvanically coupled single phases generally occurring in NdFeB-based magnets has been characterized in 0.5 M NaCl solution with pH 8.4. Electrochemical characterization of multiphase nanocrystalline hot pressed $Nd_{14}Fe_{80}B_6$ and $Nd_{12}Dy_2Fe_{73.3}Co_{6.6}Ga_{0.6}B_{5.6}$ magnets has been also established. Based on the results presented in this study, the following conclusions can be drawn:

(i) The Nd-rich phase dissolves actively, while the B-rich phase and the ferromagnetic (ϕ)-phase suffer from pitting corrosion with anodic polarization. The order of corrosion sensitivity of the uncoupled single phases is: ϕ-phase < B-rich phase < Nd-rich phase.

(ii) The Nd-rich phase/ferromagnetic phase couple generates the highest galvanic coupling current density among all pairs of coupled phases. Upon coupling, the Nd-rich phase represents the typical anode, whereas the B-rich phase and the ferromagnetic phase act as cathodes.

(iii) Pitting corrosion initiates on Nd-rich regions at the flakes boundaries of hot pressed nanocrystalline magnets. Intergranular corrosion initiates on pit walls and propagates from them. Crystallographic tunneling seems to be a supporting process of pitting and intergranular corrosion propagation.

(iv) Co and Ga additions reduce the rate of initiation and propagation of pitting corrosion of NdFeB-based magnets due to modification of the composition of magnet phases, (i.e., intergranular phases) resulting in the reduction of the strength of the galvanic coupling effect.
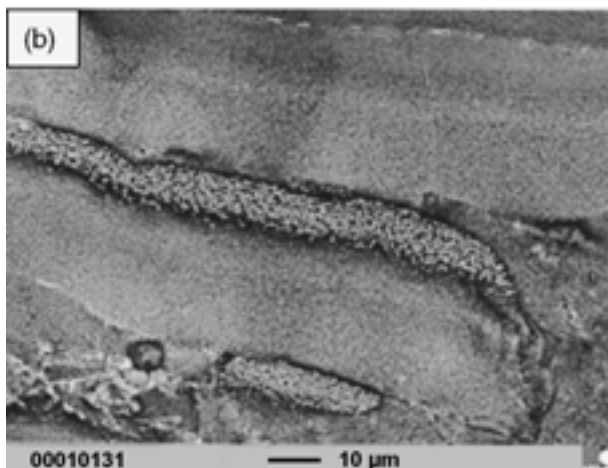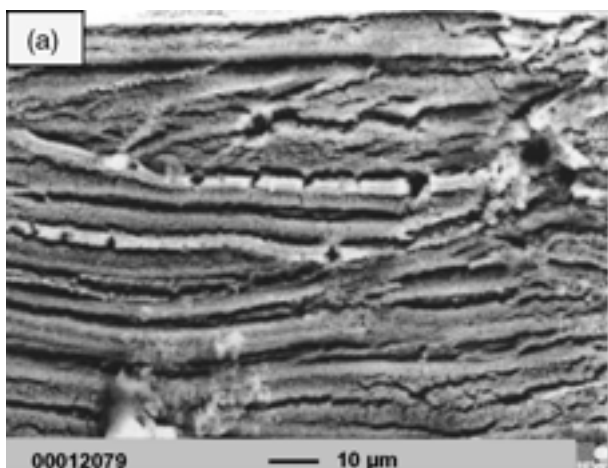
Fig. 10. SEM micrographs for (a) MQP-A and (b) MQU-G magnets surfaces after immersion in 0.001 M HCl solution for 10 min.

References

1. S. Hirosawa and Y. Kaneko, Proceedings of the 15th international workshop on 'Rare Earths and their Applications', Dresden, Germany (1998), p. 43.

2. H. Bala, G. Pawlowska, S. Szymura, V.V. Sergeev and Yu.M. Rabinovich, *J. Magn. Magn. Mater.* **87** (1990)1255.

3. L. Schultz, A.M. El-Aziz, G. Barkleit and K. Mummert, *Mater. Sci. Eng.* **A267** (1999) 307.

4. G. Schneider, E-T. Hennig, G. Petzow and H. Stadelmaier, *Z. Metallkunde* **77** (1986) 755.

5. G.W. Warren, G. Gao and Q. Li, *J. Appl. Phys.* **70** (1991) 6609.

6. T.S. Chin, R.T. Chang, W.T. Tsai and M.P. Hung, *IEEE Trans. Magn.* **24** (1988) 1927.

7. H. Bala, S. Szymura and J.J. Wyslocki, *J. Mater. Sci.* **25** (1991) 571.

8. K. Sugimoto, T. Sohma, T. Minowa and M. Honshima, Japan Metal Society Fall Meeting, (1987), p. 604.

9. H. Bala, G. Pawlowska, S. Szymura and Yu.M. Rabinovich, *Br. Corros. J.* **33** (1998) 37.

10. A.A. El-Moneim, A. Gebert, F. Schneider, O. Gutfleisch and L. Schultz, *Corros. Sci.* **44** (2002) 1097.

11. A.A. El-Moneim, A. Gebert, M. Uhlemann, O. Gutfleisch and L. Schultz, *Corros. Sci.* **44** (2002) 1857.

12. A.A. El-Moneim, O. Gutfleisch, A. Plotnikov and A. Gebert, *J. Mag. Mag. Mater.* **248** (2002) 121.

13. A. Gebert, A.A. El-Moneim, O. Gutfleisch and L. Schultz, *IEEE Trans. Magn.* **38** (2002) 2979.

14. G. Pawlowska, PhD thesis, Polytechnica of Czestochowa, Poland (1996).

15. H.P. Hack, 'Galvanic Corrosion-Test Methods' (NACE International, 1993).

16. A. Igual-Munoz, J. Carcia-Anton, J.L. Guinon and V. Perez-Herranz, *Corrosion* **57** (2001) 516.

17. L. Li and C.D. Graham, Jr, *J. Appl. Phys.* **67** (1992) 2130.

18. L. Li, PhD thesis, University of Pennsylvania (1992).

19. A. Kirchner, W. Grünberger, O. Gutfleisch, V. Neu, K-H Müller and L. Schultz, Proceedings of the 15th international workshop on 'Rare Earths and their Applications', Dresden, Germany, (1998), p. 373.

20. S. Szymura, H. Bala, G. Pawlowska, Yu.M. Rabinovich, V.V. Sergeev and D. Pokrovskii, *J. Less Common Metals* **175** (1991)185.

21. H. Yamamoto, S. Hirodawa, S. Fujimura, K. Tokuhara, H. Nagata and M. Sagawa, *IEEE Trans. Magn.* **23** (1987) 2100.

22. J. Fidler, *IEEE Trans. Magn.* **21** (1985) 1955.

23. J.S. Bendat and A.G. Piersol, 'Random Data: Analysis and Measurement Procedures' (Wiley-Interscience, New York, 1971).

24. F. Mansfeld and H. Xiao, *J. Electrochem. Soc.* **140** (1993) 2205.

25. G. Barkleit, A.M. El-Aziz, F. Schneider and K. Mummert, *Mater. Corros.* **52** (2001) 193.

26. H.P. Leckie and H.H. Uhlig, *J. Electrochem. Soc.* **113** (1966) 1262.

27. Z. Szklarska Smialowska, 'Pitting Corrosion' (NACE, 1986).

28. K.E. Heusler and L. Fischer, *Mater. Corros.* **27** (1976) 551.

29. M. Pourbaix, 'Atlas of Electrochemical Equilbria in Aqueous Solution' (Pergamon, oxford, 1966).

30. D.E. Williams, C. Wetscott and M. Fleischmann, *J. Electrochem. Soc.* **132** (1985) 1804.

31. D.E. Williams and C. Wetscott, M. Fleischmann, *J. Electrochem. Soc.* **132** (1985) 1796.